Supporting Information

Additive-free Red Phosphorus/$Ti_3C_2T_x$ MXene Nanocomposites Anodes for Metal-ion Batteries

Chandrasekar M Subramaniyam[1,2], Min-A Kang[1], Jian Li[1], Armin VahidMohammadi[3], Mahiar Max Hamedi[1,2*]

[1] *Department of Fibre and Polymer Technology, School of Engineering Sciences in Chemistry, Biotechnology and Health, KTH Royal Institute of Technology, 100 44 Stockholm, Sweden*

[2] *Wallenberg Wood Science Center, Teknikringen 56-58, SE-100 44 Stockholm, Sweden*

[3] *Department of Materials Science and Engineering, A.J. Drexel Nanomaterials Institute, Drexel University, Philadelphia, Pennsylvania, United States*

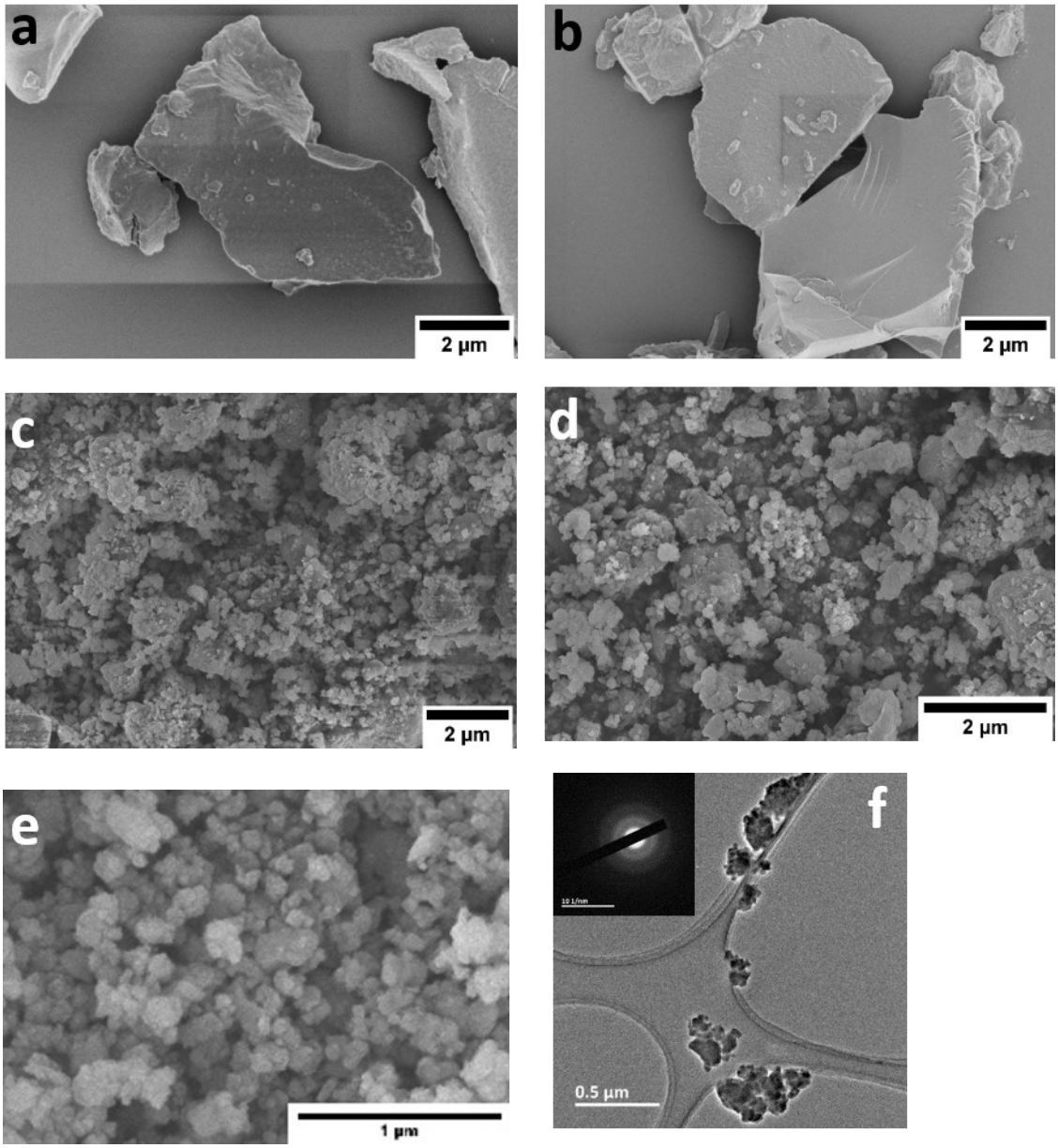

Figure S1 (a, b) FESEM shows the morphology of bulk RP and (c, d) represents that of as-ball-milled RP powders. The bulk RP chunks are rigid and are of few 10s of micron. Upon ball milling of these bulk RP at 300 rpm for 150 mins under inert atmosphere resulted in ultra-fine particles clustered together as micron particles: (e) FESEM depicts the uniform distribution of ball milled RP nanoparticles; TEM images show well dispersed RP nanoparticles (f) with corresponding (insert) SAED pattern exhibiting its amorphous phase

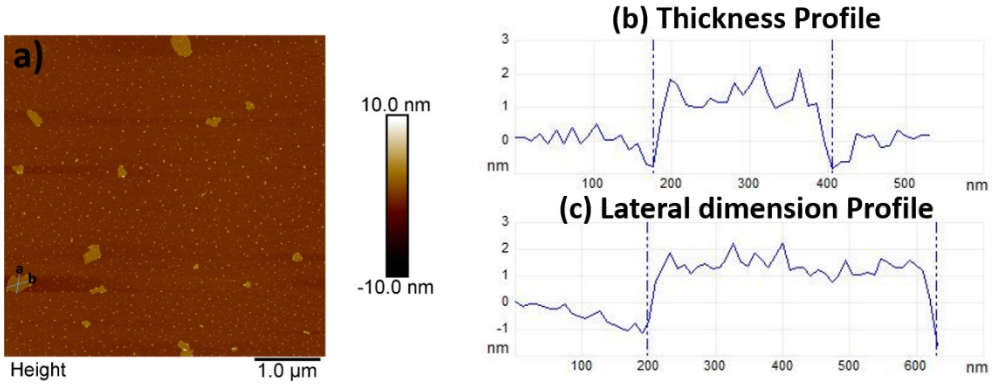

Figure S2 (a) AFM images of MXene nanosheets whose thickness is 2-3 nm (b) and lateral dimension are of 200-400 nm (c).

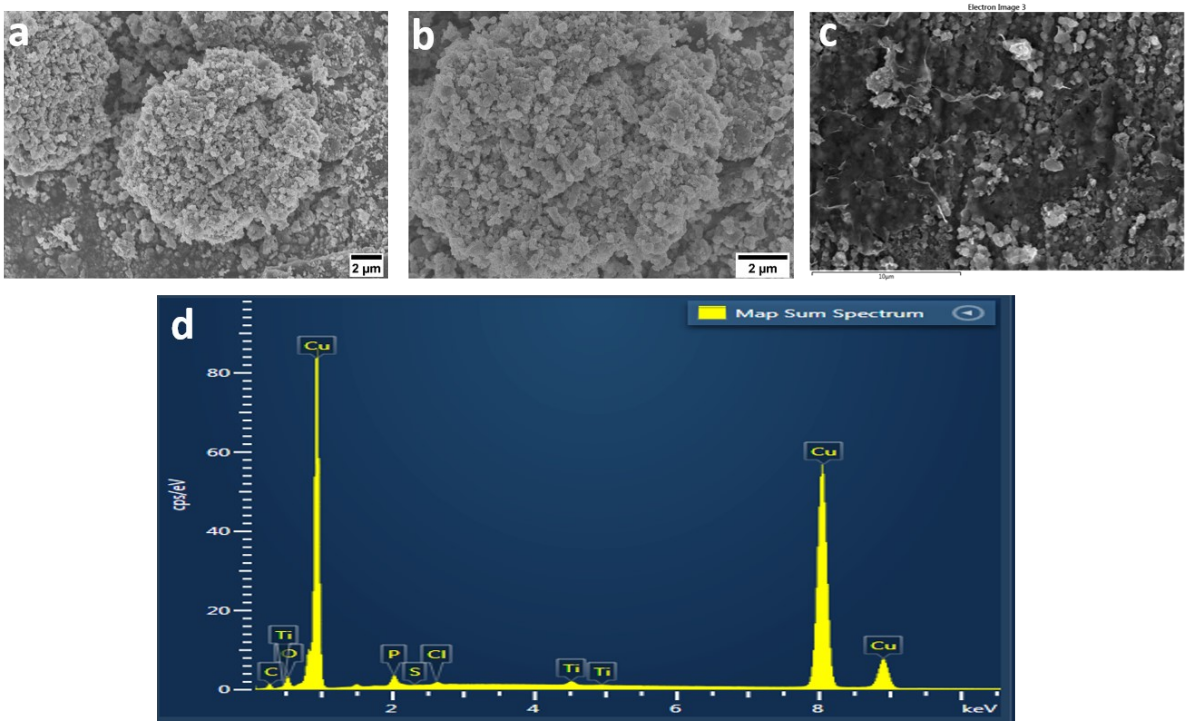

Figure S3 (a, b) FESEM shows the RP nanoparticles are dispersed over rGO sheets which were then stacked layered in-between MXene nanosheets (c) and corresponding EDS mapping of RP-rGO/MXene (d).

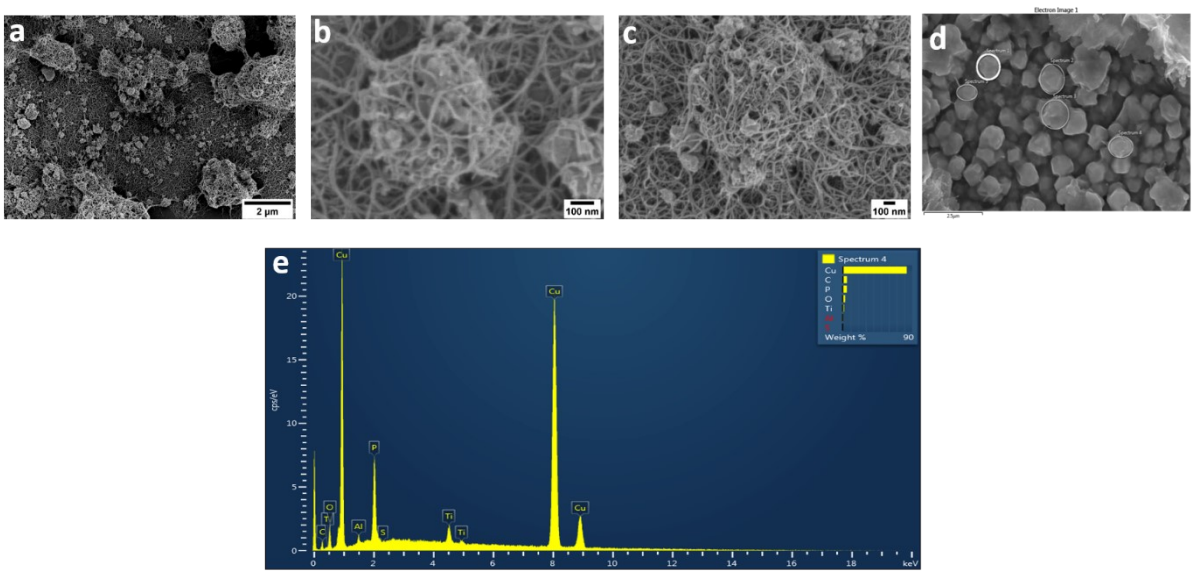

Figure S4 (a, b) FESEM shows flexible 1D MWCNT helped completely engulf the RP nanoparticles providing enhanced particle-to-particle interconnectivity when blended with MXene ink (d) and corresponding EDS mapping of RP-MWCNT/MXene (e)

Detail of XPS Calculations

Table S1: Relative amounts with total P 2p as 100%

Sample	Atomic %	P 2p (tot = 100 %)		
	P_{tot}	P_{tot}	P-P 130 eV	P-O 133-135 eV
MXene	0.6	100	-	100
RP/ MXene	5.4	100	27	73
RP-rGO/ MXene	4.7	100	14	86
RP-MWCNT/ MXene	2.7	100	10	90

The tables below are from the report, now shown with 2 decimals to use for the calculations:

Table S1a:

Relative surface composition in atomic %, quantified from XPS detail spectra.

Sample	**Atomic %**										
Substrate surface: Si wafer	**C**	**O**	**Ti**	**P**	**Cu**	**Si**	**F**	**N**	**Cl**	**S**	**Zr**
RP-MWCNT/ MXene	**31.90**	**26.16**	**23.77**	**2.68**	**-**	**0.40**	**11.80**	**1.16**	**2.13**	**-**	**-**

Curve-fitted carbon spectra - Table S1b:

Sample	**Atomic %**	**C 1s tot = 100 %**				
	C tot	**C carbides** 282-3 eV	**C 1** 285.0 eV	**C 2** 286.5-6 eV	**C 3** 287.9-288.1 eV	**C 4** 289.2-3 eV
RP-MWCNT/ MXene - Si wafer	**31.90**	45.43	30	17	5	3

If assume that all carbides detected are Ti-C, that means from above:
45.43% x 31.90 atomic% C = 14.49 atomic% as Ti-C.

How much of the total Ti peak is then Ti-C?
14.49 atomic% Ti-C / 23.77 atomic% Ti $_{total}$ = **60.96% of the total Ti 2p peak**

Curve-fitted P 2p spectra - Table S1c:

Sample	**Atomic %**	**P 2p tot = 100 %**		
	P tot	**P tot**	**P 1** 130 eV	**P 2** 133-135 eV
RP-MWCNT/ MXene - Si wafer	**2.68**	100	10	89.57

If assume that all oxidized P at about 133-135 eV are signals from Ti-O-P, that means from above:
89.57% x 2.68 atomic% C = 2.40 atomic% oxidized P (assume all is in the form of Ti-O-P).

How much of the total Ti peak is then Ti-O-P?
2.40 atomic% Ti-O-P / 23.77 atomic% Ti $_{total}$ = **10.10% of the total Ti 2p peak**

Curve-fitted O 1s spectra - Table S1d:

Sample	**Atomic %**	**O 1s tot = 100 %**		
	O tot	**O tot**	**O 1** 530-531 eV	**O 2** 532-534 eV
RP-MWCNT/ MXene - Si wafer	**26.16**	100	37.31	63

If assume that all inorganic O at about 530-1 eV are signals either from TiO_2 or Ti-O-P, that means from above:
37.31% x 26.16 atomic% C = 9.76 atomic% as inorganic oxides
Of these are 2.40 atomic% from Ti-O-P, so what remains for TiO_2 is: 9.76-2.40 atomic% =7.36 atomic%
How much of the total Ti peak is then TiO_2?
7.36 atomic% / 23.77 atomic% Ti $_{total}$ = **30.96% of the total Ti 2p peak**

We have performed curve-fit for the Medium-resolved Ti 2p spectra (sample on Si wafer, spectra 23 - sufficient to curve-fit only the Ti $2p^{3/2}$ peak) - see below – possible after the many different assumptions mentioned above.

To summarize the assumptions made:
- all carbides detected are in the form of Ti-C
- all oxidized P at about 133-135 eV are signals from Ti-O-P
- all inorganic O at about 530-1 eV are signals either from TiO_2 or Ti-O-P

For curve-fitted the following values were use:

Component	Peak positions used, (in eV) [Ref]	**Obtained peak position (eV) in this work**
Ti-C	455.4 [3]	**"good enough"**
Ti-C	455.1 [8]	455.5
Ti-O-P	456.4 [8]	456.6
TiO_2	458.6-459.3 [20]	458.2

		Values obtained – "good enough":
How much of the total Ti peak is then Ti-C?	60.96% of the Ti 2p peak	60.3 %
How much of the total Ti peak is then Ti-O-P?	10.10% of the Ti 2p peak	9.6 %
How much of the total Ti peak is then TiO_2?	30.96% of the Ti 2p peak	30.2 %

Total: 102 %, so aimed for slightly lower values

Medium resolved Ti 2p spectra: Ti 2p:23 (RP_MWCNT_MXene)

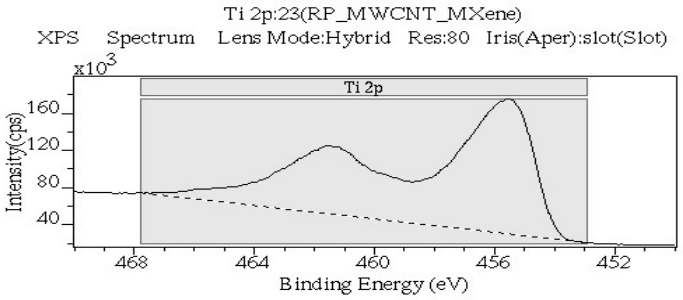

Curve-fit of three peaks corresponding to Ti-O, Ti-C and Ti-O-P:

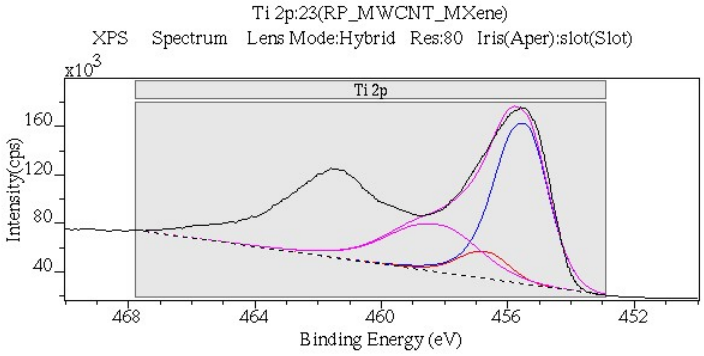

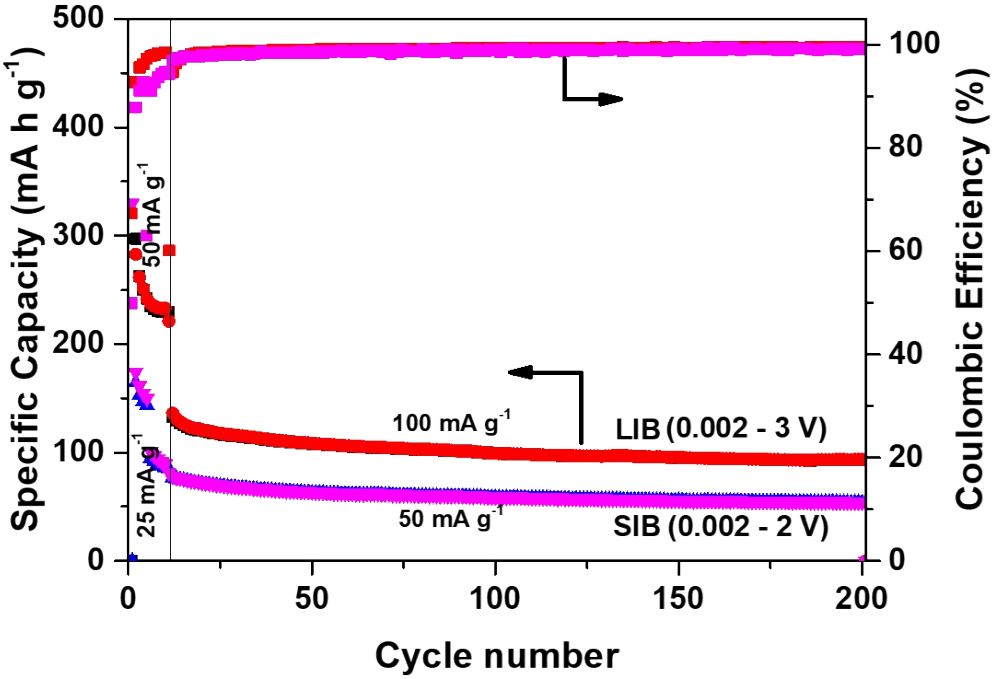

Figure S5 Electrochemical performance of MXene as anode for: (1) LIB cycled between 0.002 – 3 V using 1 M $LiPF_6$ in 1:1 (*v/v*) EC:DEC electrolyte; (2) SIB cycled between 0.002 – 2 V using 1 M $NaPF_6$ in 1:1 (*v/v*) EC:DEC + 10 vol.% FEC electrolyte.

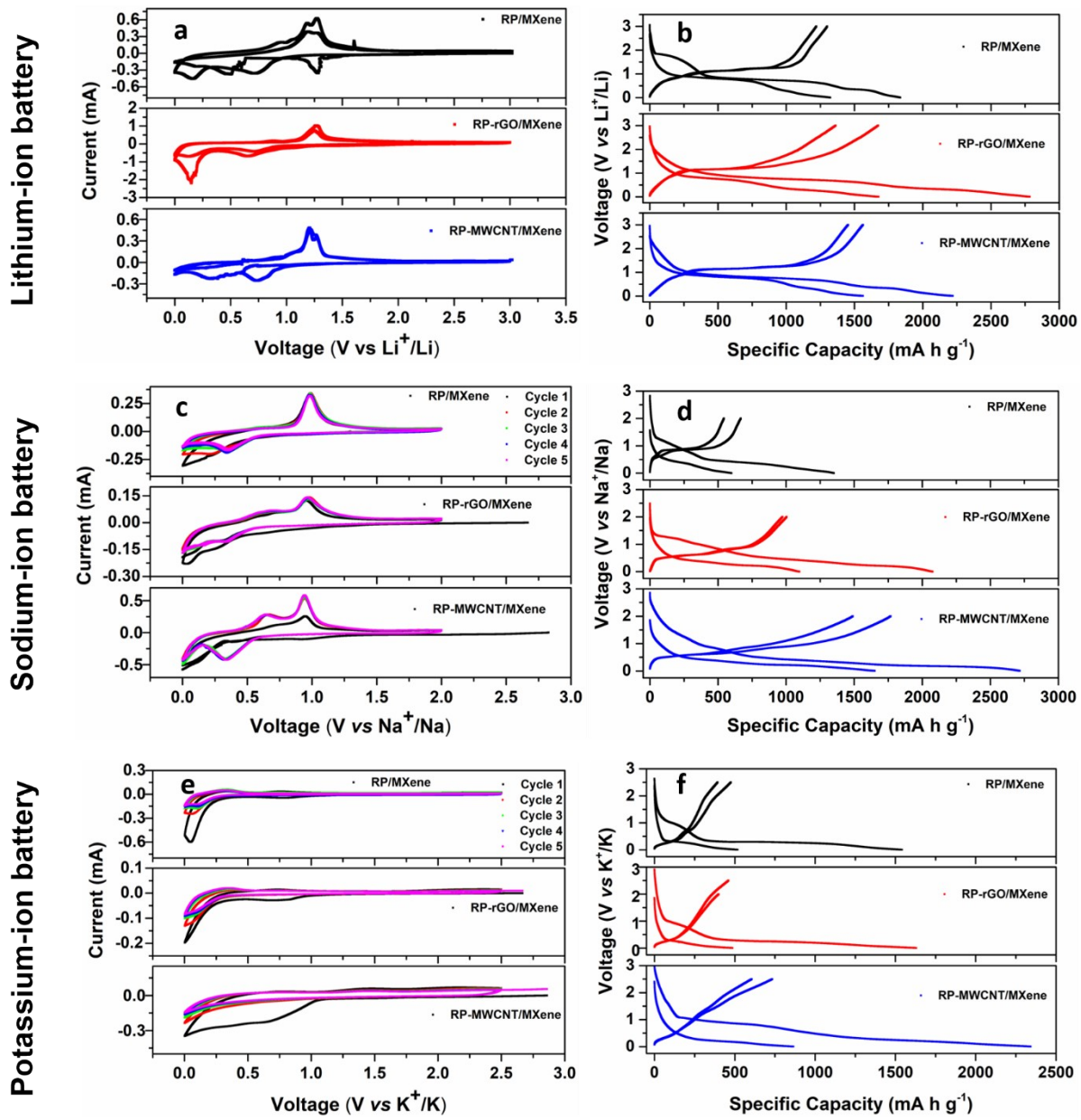

Figure S6 Electrochemical performance of RP composites as anode for LIB, SIB and KIB (a,c,e) cyclic voltammetry of 5 cycles obtained at 0.1 mV s^{-1}; (b,d,f) charge-discharge of 1st & 2nd cycles 50 mA g^{-1}.

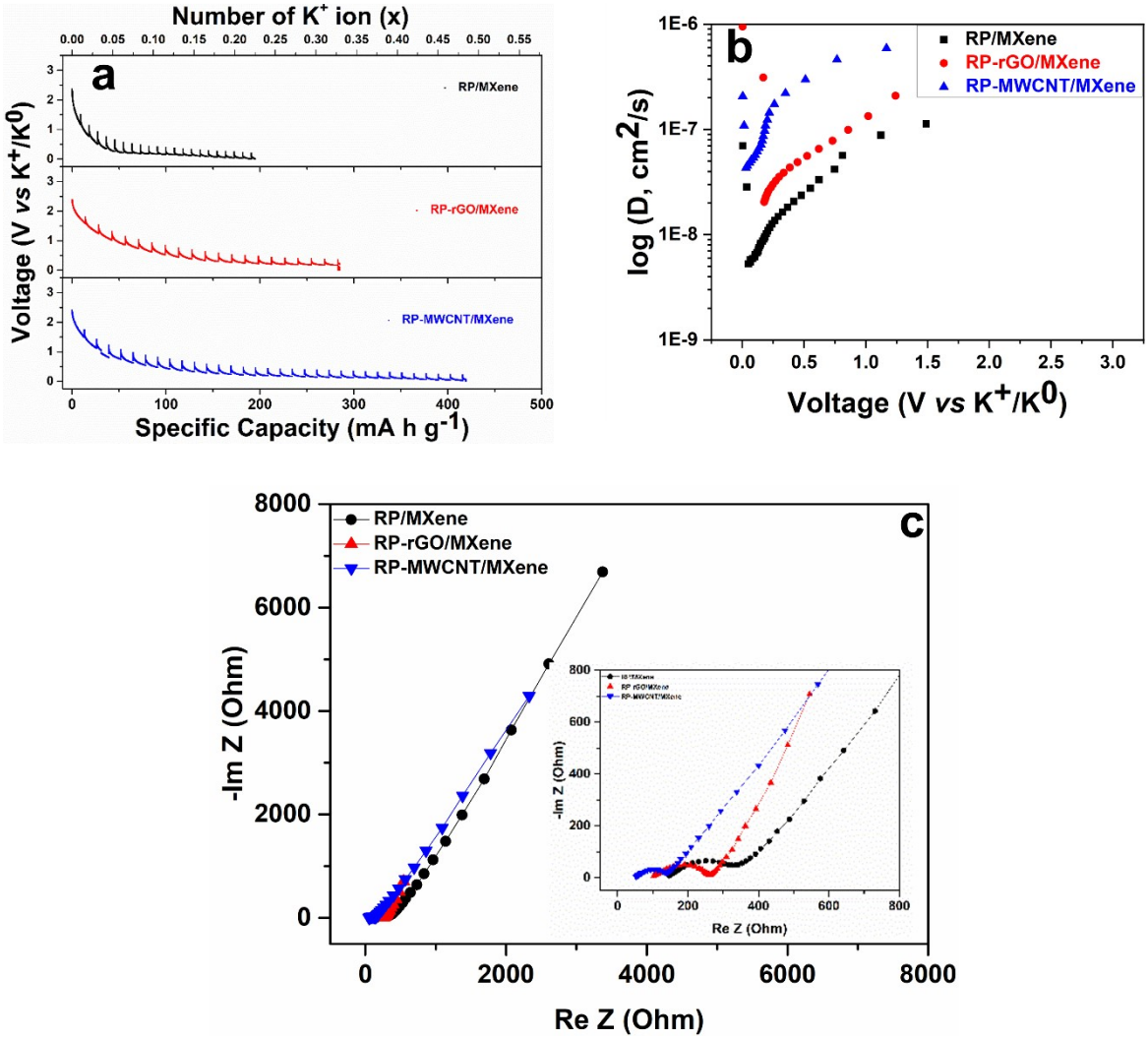

Figure S7a,b GITT discharge plot and corresponding K^+ chemical diffusion coefficient in the composites at various voltage. GITT was measured after 2nd charge-discharge cycles to evade the effect of solid-electrolyte-interface formed during first cycle. (c) Nyquist plot of electrochemical-impedance-spectroscopy (EIS) of fresh KIBs of various composites.

Table S2: Comparative electrochemical performance of additive-free RP-MXene electrodes for lithium-ion and Sodium-ion batteries with literature reports

Lithium-ion battery								
Synthesis, Morphology	**Wt.% P in composite**	**Resistance to charge transfer (R_{ct}, Ohm)**	**Potential (V vs Li^+/Li)**	**Current rate (mA g^{-1})**	**Initial capacity (Discharge/ Charge) (mA h g^{-1})**	**Capacity retention (mA h g^{-1})/ (cycles) current density (mA g^{-1})**	**Rate test (mA g^{-1}), (cycle)/ capacity (mA h g^{-1})**	**Ref.**
Binder-free electrodes prepared by hand blending of RP nanoparticle with low dimensional carbonaceous materials in viscous and conducting MXene ink	***~50.0 - 70.0***	***55***	***0.02 – 3.0***	***50***	**2784/ 1673.1**	**1077.6 (500) 260 263.3 (10000)2600**	**500 (100) 1293.7**	***Present work***
Ball milling of RP and $Ti_3C_2T_x$ powders in NMP solvent at 1000 rpm for 40 mins.	29.5	~200	0.00 – 3.0	50	906	~585.3 (1000) 200	1000 (5) 197	[9]
$Ti_3C_2T_x$/CNTs@P nanohybrid by loading red P into a $Ti_3C_2T_x$/CNT hybrid network *via* a ball-milling method	~50.0	50.11	0.01 – 3.0	50	2598	2078 (500) 50	78k (5) 454	[3]
chemical vapor deposition method to prepare walnut-like structure N-doped $Ti_3C_2T_x$ MXenes/P	27.17	~150	0.01 – 3.0	100	1160.4/666.5	2499 (1000) 500	2000 (5) ~350	[6]

composites (N– $Ti_3C_2T_x$ /P)								
Black phosphorus quantum dots/ Ti_3C_2 MXene composites	12.0	~160	0.005 – 3.0	50	1730	520 (2400) 1000	167 (2000) 10	[4]
Sodium-ion battery								
Morphology Synthesis Method	**Wt.% P in composite**	**Resistance to charge transfer (R_{ct}, Ohm)**	**Potential (V vs Na^+/Na)**	**Current rate (mA g^{-1})**	**Initial capacity (Discharge/ Charge) (mA h g^{-1})**	**Capacity retention (mA h g-1)/ (cycles) current density (mA g-1)**	**Rate test (mA g-1), (cycle)/ capacity (mA h g^{-1})**	**Ref.**
Binder-free electrodes prepared by hand blending of RP nanoparticle with low dimensional carbonaceous materials in viscous and conducting MXene ink	***~50.0 - 70.0***	***541.2***	***0.01 – 2.0***	***50***	**2716.2/ 1767.8**	**371.6 (100) 500**	**193.3 (2000) 10**	***Present work***
Ball milling of RP and $Ti_3C_2T_x$ powders in NMP solvent at 1000 rpm for 40 mins.	29.5	-	0.00 – 2.5	50	863.8	370.2 (200) 50	-	[9]
Black phosphorus quantum dots/ Ti_3C_2 MXene composites	12	~1300	0.005 – 3.0	50	~723	~<100 (1000) 1000	~<100 (2000) 10	[4]
RP assisted ball-milling of $Ti_3C_2T_x$ nanodot composite	40	-	***0.01 – 2.0***	100	~1500	~1000 (150) 100	750 (1000) 5	[7]
Black phosphorus/ Ti_3C_2 MXene nanocomposite by	16.67	-	0.01 – 3.0	100	1280/ 661.9	80 (100) 500	67.3 (1000) 5	[10]

ball-milling method								
PDDA/Black phosphorus and Ti_3C_2 MXene Heterostructures	38.4	127.6	0.01 – 3.0	100	2588/ 1780	658 (2000) 1000	461 (2000) 5	[8]
2D Phosphorene/ $Ti_3C_2T_x$ MXene Nanoarchitecture	19.6	-	0.00 – 3.0	100	845/ 533	467 (100) 100	266 (2000) 5	[11]

Potassium-ion battery

Morphology Synthesis Method	**Wt.% P in composite**	**Resistance to charge transfer (R_{ct}, Ohm)**	**Potential (V vs Li^+/Li)**	**Current rate (mA g^{-1})**	**Initial capacity (Discharge/ Charge) (mA h g^{-1})**	**Ref.**
Binder-free electrodes prepared by hand blending of RP nanoparticle with low dimensional carbonaceous materials in viscous and conducting MXene ink	***~50.0 - 70.0***	***93.24***	***0.01 – 2.5***	***50***	**2341.6/ 732.8**	***Present work***
Confine nanoscaled red P within a porous carbon structure	~52	-	0.01 – 2.0	20	706/ 416	[12]
Phosphorus/carbon composite, obtained by a ball-milling	~20	-	0.001 – 3.0	20	1678.4/ 795.2	[13]
Red Phosphorus Nanoparticle@3D Interconnected Carbon Nanosheet	~63.9	1354	0.01 – 2.0	100	1212/ 715.2	[14]
Black phosphorus/ Graphite composite by ball milling	~50	-	0.01 – 2.0	50	~900/617	[15]
Red phosphorus/ Carbon composite by ball milling	~36	-	0.01 – 2.5	25	914.8/ 624.5	[16]

RP/ carbon nanotube-backboned mesoporous carbon by vapor condensation technique	~40	-	0.01 – 2.0	50	772.8/ 490.9	[17]

Note: Table compares the Electrochemical performance of present work with the available reported (Red or Black) P - MXene based composite literatures.

(1) We reported the highest active RP loading of ~50 - 70 wt.% in the additive-free MXene electrodes as compared to other reports as negative electrodes for MIBs (M = Li, Na, K).

(2) Our works shows highest initial discharge and charge capacity, respectively, for LIB (2784 and 1673.1 mA h g^{-1}), SIB (2716.2 and 1767.8 mA h g^{-1}) as compared to others reported.

(3) The present works outclassed other reports in term of capacity retention of 1077.6 mA h g^{-1} at 500 mA g^{-1} for 500 cycles and 263.3 mA h g^{-1} at 2600 mA g^{-1} (1 C) for 10000 cycles for LIB anode.

(4) We are the first to report MXene based composite as anode for KIB with highest discharge and charge capacity of 2341.6 and 732 mA h g^{-1}, respectively, compared to RP-carbon based electrodes. The electrode suffered fast capacity fade in the long run maybe due to high volume change (~400 %) during discharge-charge process. Further study is required to mitigate this loss so as to harness high energy density KIB.

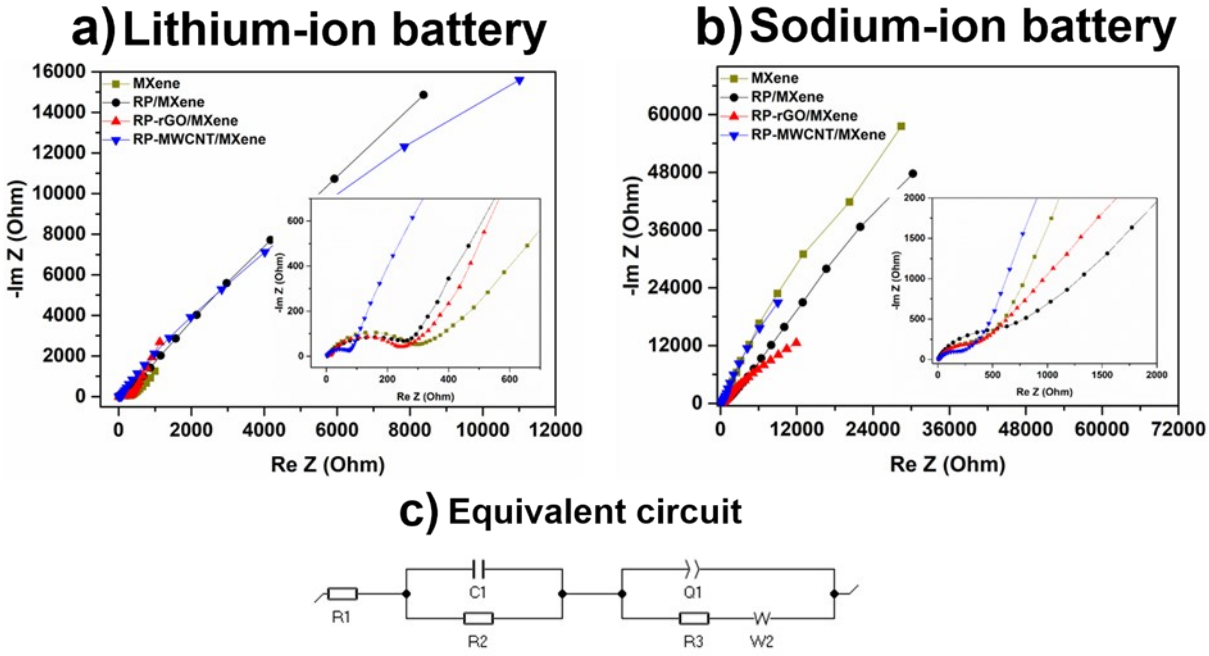

Figure S8 Nyquist plot of electrochemical-impedance-spectroscopy (EIS) of fresh MIBs: (a) LIB; (b) SIB and (c) their equivalent circuit.

Table S3 Electrochemical Impedance values of Nanocomposites for various MIBs

MIBs	**LIB**			**SIB**			**KIB**		
Nanocomposites	**R_s (Ohm)**	**R_{ct} (Ohm)**	**C_{dl} (µF)**	**R_s (Ohm)**	**R_{ct} (Ohm)**	**C_{dl} (µF)**	**R_s (Ohm)**	**R_{ct} (Ohm)**	**C_{dl} (µF)**
MXene	10.71	257.0	9.88	7.85	381.10	197.0	-	-	-
RP/MXene	5.53	311.0	6.74	7.09	641.25	52.7	146.3	589.0	43.5
RP-rGO/MXene	3.73	77.0	2.20	5.44	621.30	12.8	101.4	167.3	23.3
RP-MWCNT/MXene	2.61	55.0	4.58	4.90	541.20	24.6	51.5	93.24	13.5

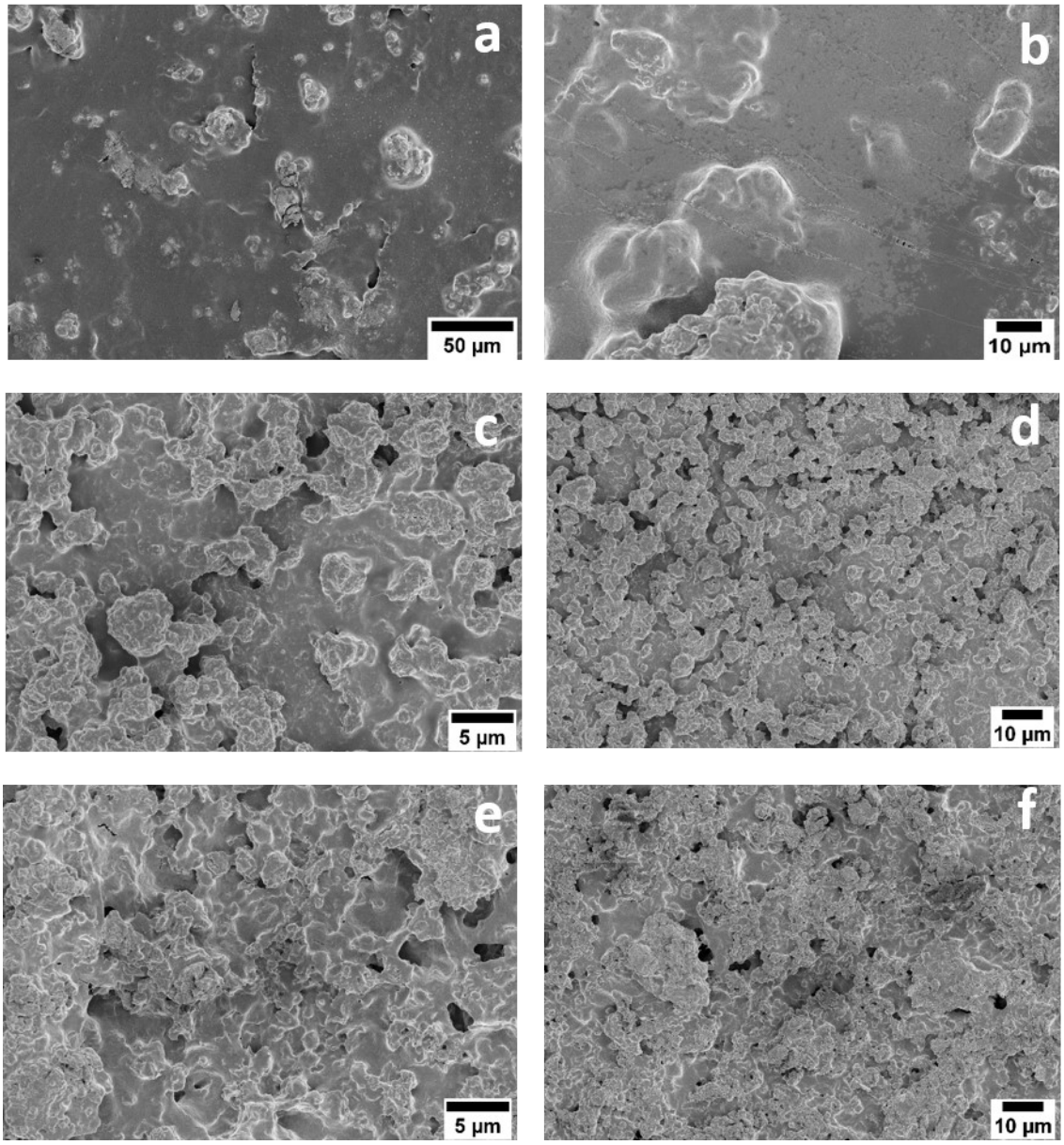

Figure S9 FESEM morphological analysis of electrodes after cycling as anode for LIBs: (a,b) RP-MWCNT/MXene after 10000 cycles; (c,d) RP-rGO/MXene after 100 cycles and (e,f) RP/MXene after 100 cycles.

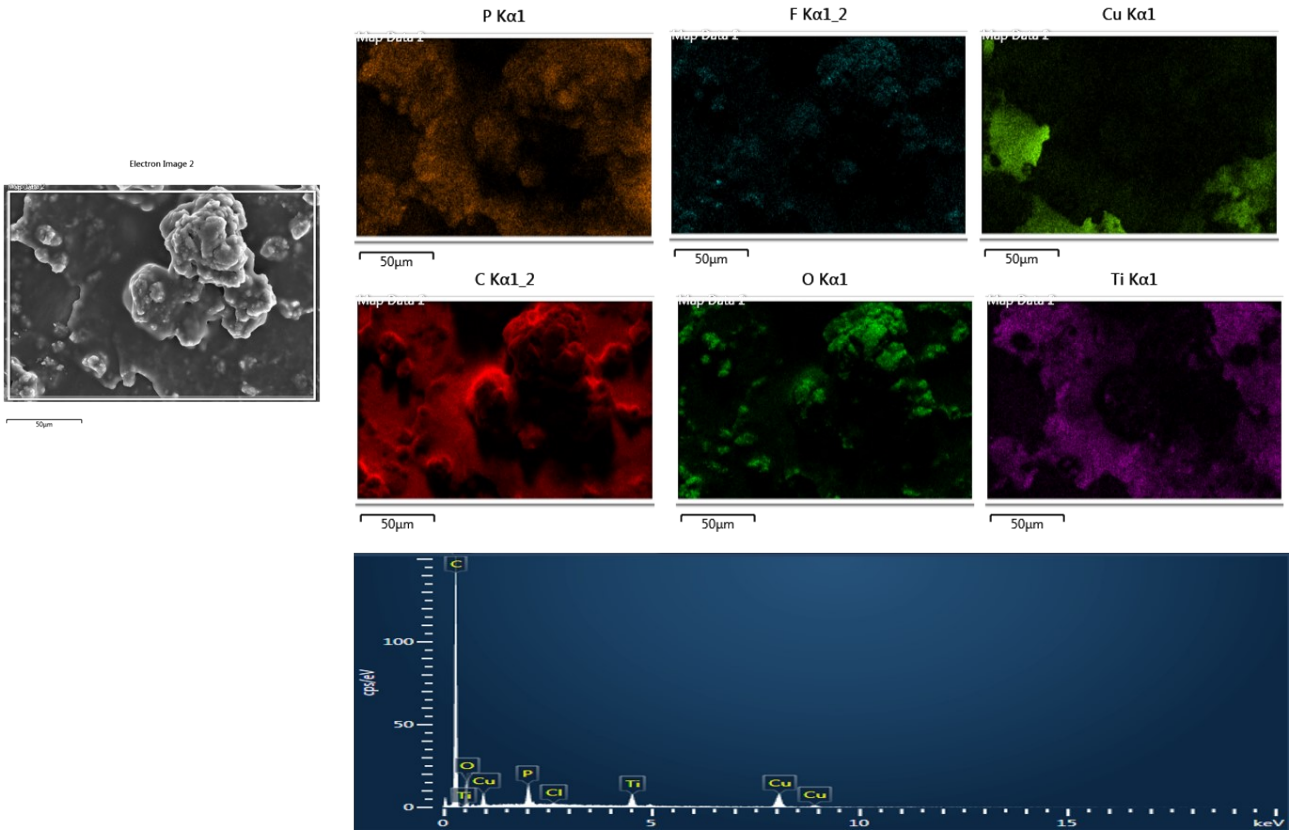

Figure S10 Elemental composition of RP-MWCNT/MXene after 10000 LIB cycles.

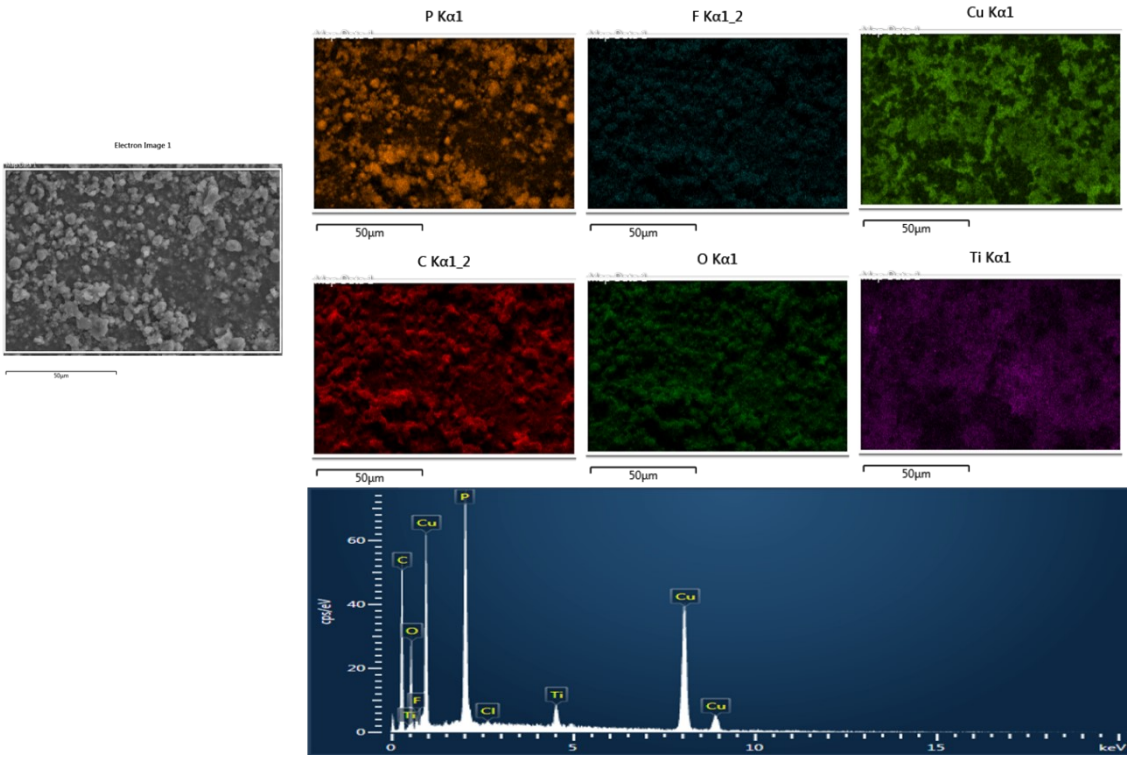

Figure S11 Elemental composition of RP/MXene after 100 LIB cycles.

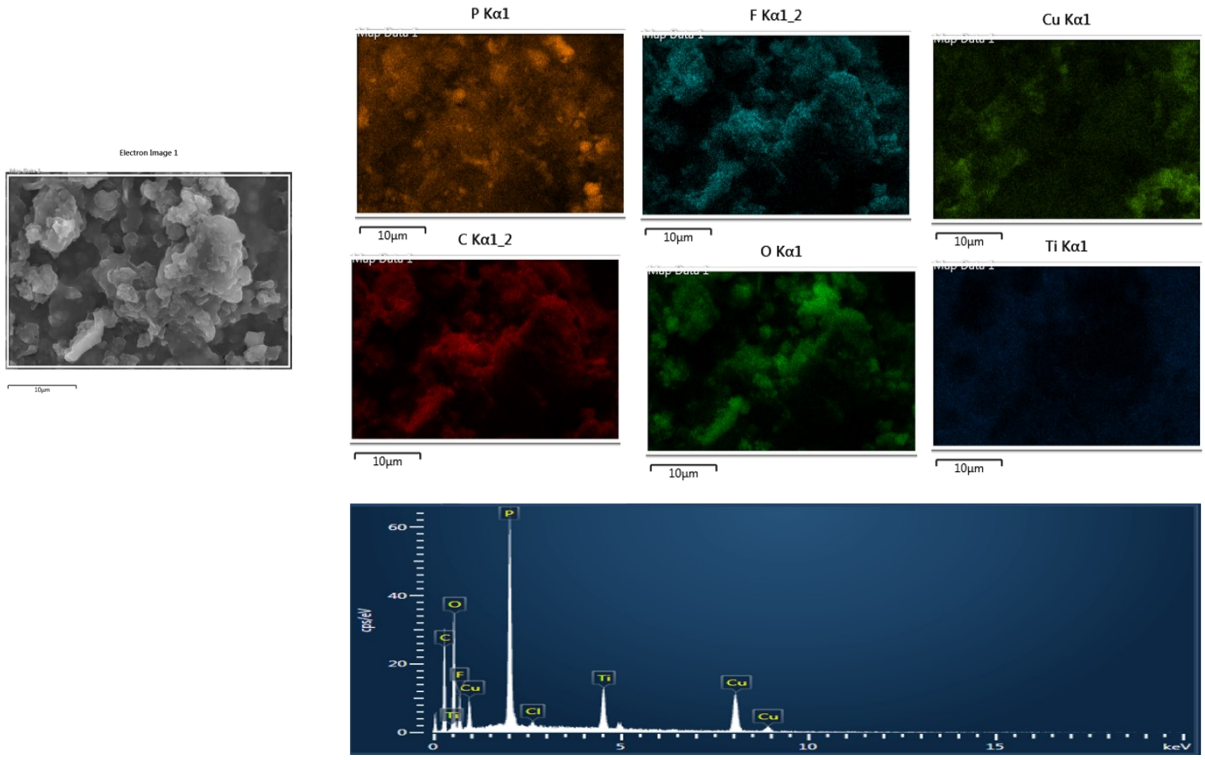

Figure S12 Elemental composition of RP-rGO/MXene after 100 LIB cycles.

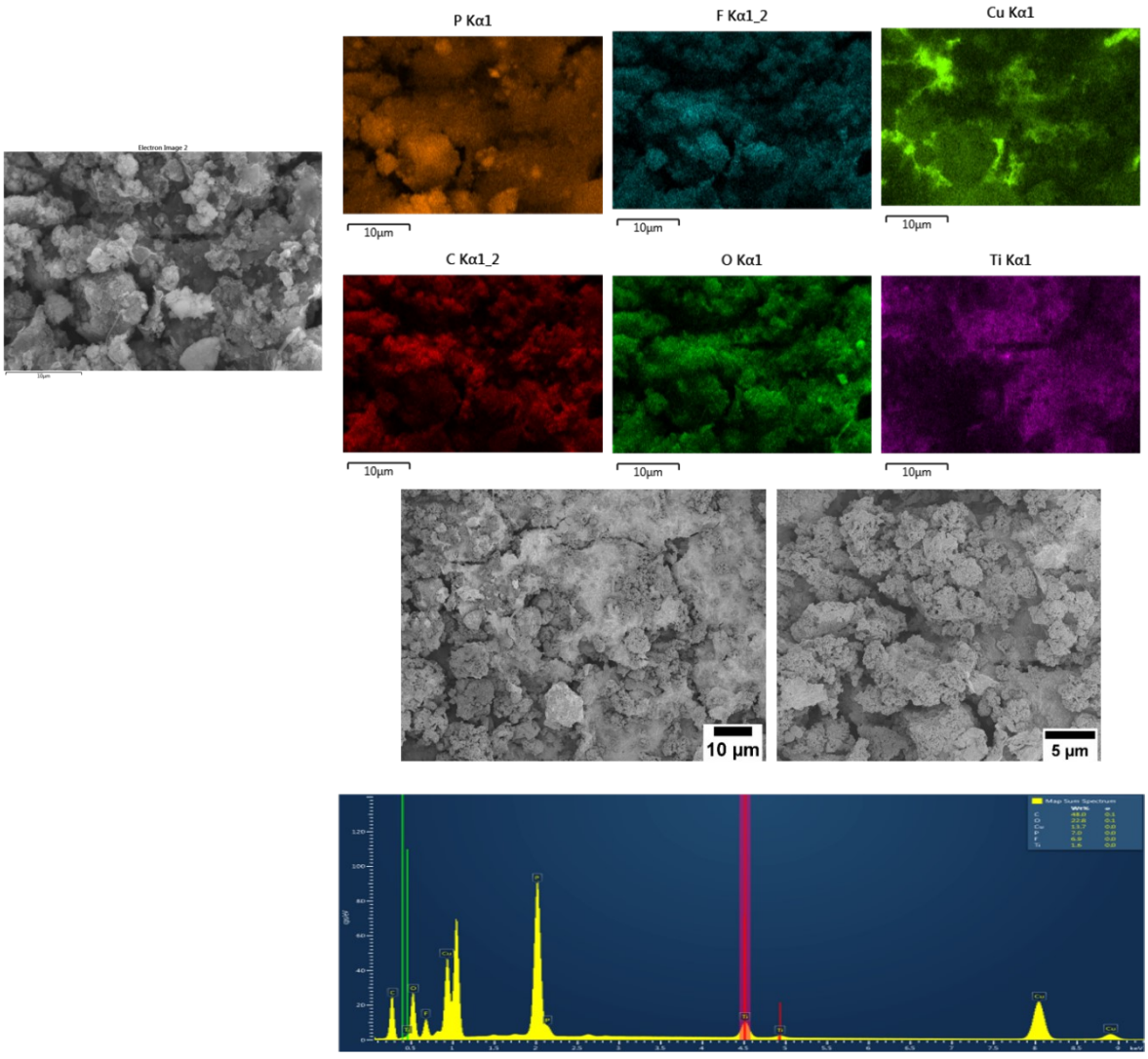

Figure S13 Morphological and elemental composition of RP/MXene after 100 SIB cycles.

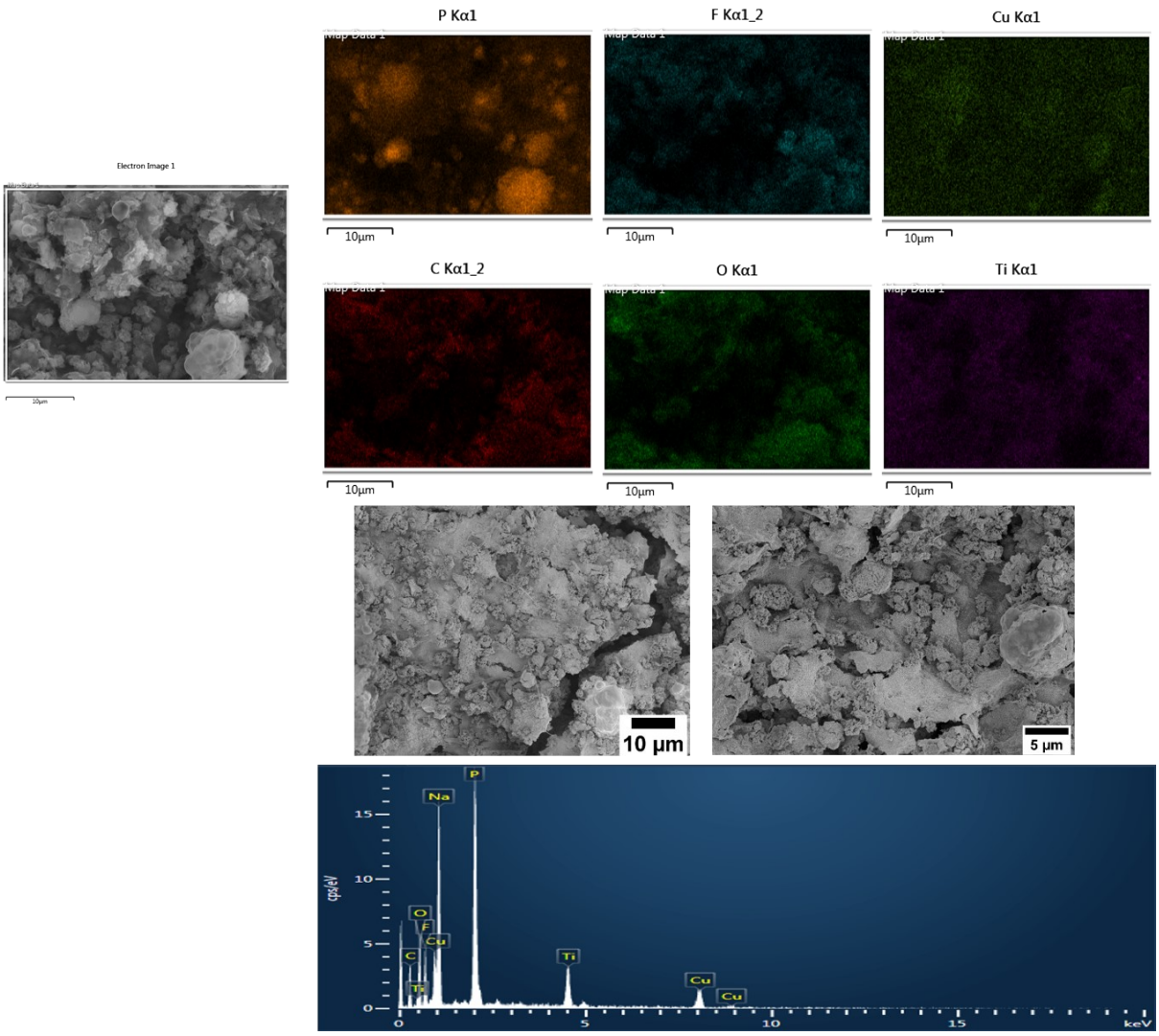

Figure S14 Morphological and elemental composition of RP-rGO/MXene after 100 SIB cycles.

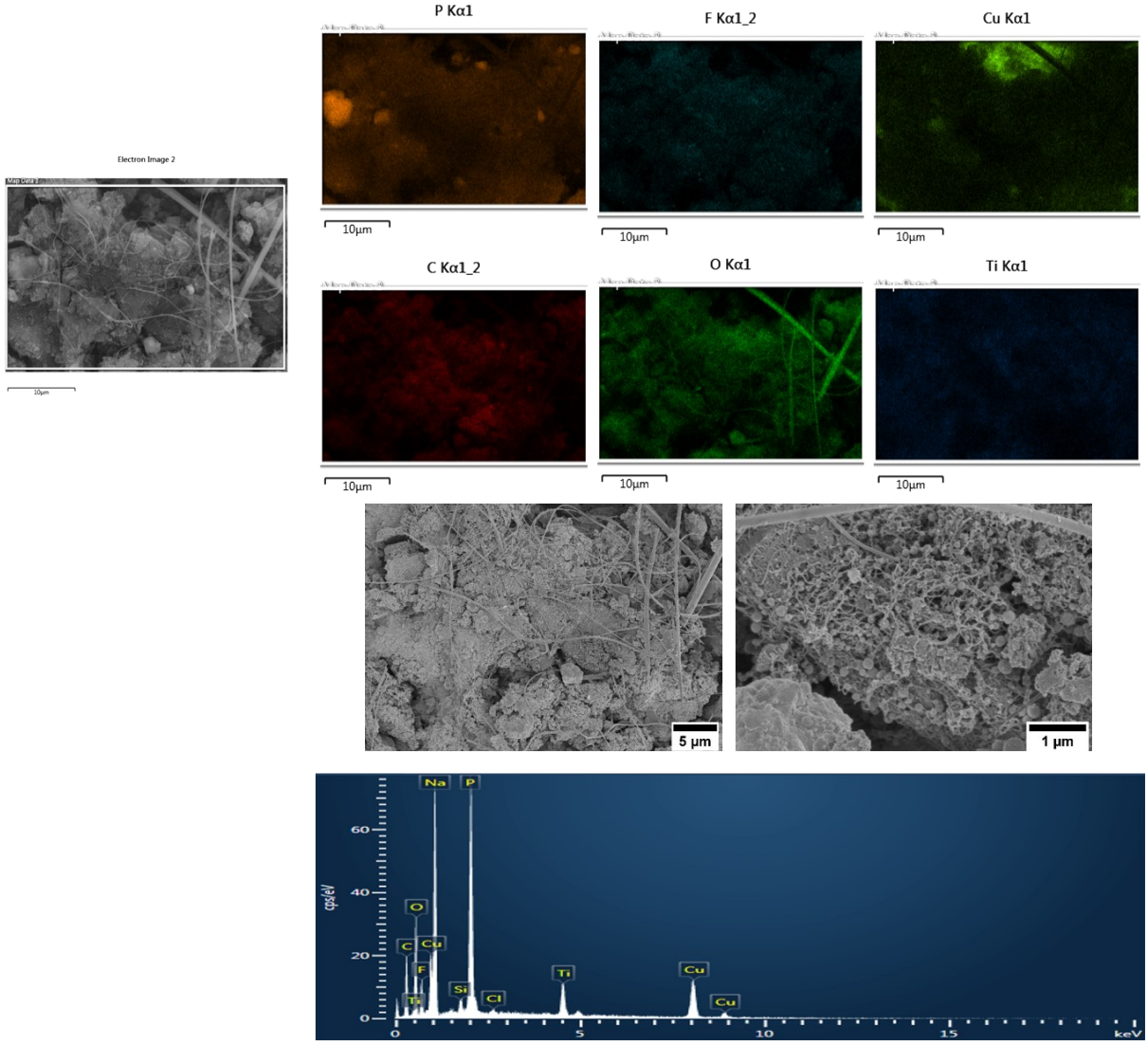

Figure S15 Morphological and elemental composition of RP-MWCNT/MXene after 100 SIB cycles.

References

[1] A. Sarycheva, Y. Gogotsi, Raman Spectroscopy Analysis of the Structure and Surface Chemistry of Ti3C2Tx MXene, Chemistry of Materials, 32 (2020) 3480-3488.

[2] C.M. Subramaniyam, Z. Tai, N. Mahmood, D. Zhang, H.K. Liu, J.B. Goodenough, S.X. Dou, Unlocking the potential of amorphous red phosphorus films as a long-term stable negative electrode for lithium batteries, Journal of Materials Chemistry A, 5 (2017) 1925-1929.

[3] S. Zhang, H. Liu, B. Cao, Q. Zhu, P. Zhang, X. Zhang, R. Chen, F. Wu, B. Xu, An MXene/CNTs@P nanohybrid with stable Ti–O–P bonds for enhanced lithium ion storage, Journal of Materials Chemistry A, 7 (2019) 21766-21773.

[4] R. Meng, J. Huang, Y. Feng, L. Zu, C. Peng, L. Zheng, L. Zheng, Z. Chen, G. Liu, B. Chen, Y. Mi, J. Yang, Black Phosphorus Quantum Dot/Ti3C2 MXene Nanosheet Composites for Efficient Electrochemical Lithium/Sodium-Ion Storage, Advanced Energy Materials, 8 (2018) 1801514.

[5] S.A. Ansari, M.H. Cho, Highly Visible Light Responsive, Narrow Band gap TiO2 Nanoparticles Modified by Elemental Red Phosphorus for Photocatalysis and Photoelectrochemical Applications, Scientific Reports, 6 (2016) 25405.

[6] S. Zhang, H. Ying, R. Guo, W. Yang, W.-Q. Han, Vapor Deposition Red Phosphorus to Prepare Nitrogen-Doped Ti3C2Tx MXenes Composites for Lithium-Ion Batteries, The Journal of Physical Chemistry Letters, 10 (2019) 6446-6454.

[7] T. Zhang, X. Jiang, G. Li, Q. Yao, J.Y. Lee, A Red-Phosphorous-Assisted Ball-Milling Synthesis of Few-Layered Ti3C2Tx (MXene) Nanodot Composite, ChemNanoMat, 4 (2018) 56-60.

[8] R. Zhao, Z. Qian, Z. Liu, D. Zhao, X. Hui, G. Jiang, C. Wang, L. Yin, Molecular-level heterostructures assembled from layered black phosphorene and Ti3C2 MXene as superior anodes for high-performance sodium ion batteries, Nano Energy, 65 (2019) 104037.

[9] S. Zhang, X.-Y. Li, W. Yang, H. Tian, Z. Han, H. Ying, G. Wang, W.-Q. Han, Novel Synthesis of Red Phosphorus Nanodot/Ti3C2Tx MXenes from Low-Cost Ti3SiC2 MAX Phases for Superior Lithium- and Sodium-Ion Batteries, ACS Applied Materials & Interfaces, 11 (2019) 42086-42093.

[10] H. Li, A. Liu, X. Ren, Y. Yang, L. Gao, M. Fan, T. Ma, A black phosphorus/Ti3C2 MXene nanocomposite for sodium-ion batteries: a combined experimental and theoretical study, Nanoscale, 11 (2019) 19862-19869.
[11] X. Guo, W. Zhang, J. Zhang, D. Zhou, X. Tang, X. Xu, B. Li, H. Liu, G. Wang, Boosting Sodium Storage in Two-Dimensional Phosphorene/Ti3C2Tx MXene Nanoarchitectures with Stable Fluorinated Interphase, ACS Nano, 14 (2020) 3651-3659.
[12] K. Fang, D. Liu, X. Xiang, X. Zhu, H. Tang, D. Qu, Z. Xie, J. Li, D. Qu, Air-stable red phosphorus anode for potassium/sodium-ion batteries enabled through dual-protection design, Nano Energy, 69 (2020) 104451.
[13] X. Wu, W. Zhao, H. Wang, X. Qi, Z. Xing, Q. Zhuang, Z. Ju, Enhanced capacity of chemically bonded phosphorus/carbon composite as an anode material for potassium-ion batteries, Journal of Power Sources, 378 (2018) 460-467.
[14] P. Xiong, P. Bai, S. Tu, M. Cheng, J. Zhang, J. Sun, Y. Xu, Red Phosphorus Nanoparticle@3D Interconnected Carbon Nanosheet Framework Composite for Potassium-Ion Battery Anodes, Small, 14 (2018) 1802140.
[15] I. Sultana, M.M. Rahman, T. Ramireddy, Y. Chen, A.M. Glushenkov, High capacity potassium-ion battery anodes based on black phosphorus, Journal of Materials Chemistry A, 5 (2017) 23506-23512.
[16] W.-C. Chang, J.-H. Wu, K.-T. Chen, H.-Y. Tuan, Red Phosphorus Potassium-Ion Battery Anodes, Advanced Science, 6 (2019) 1801354.
[17] D. Liu, X. Huang, D. Qu, D. Zheng, G. Wang, J. Harris, J. Si, T. Ding, J. Chen, D. Qu, Confined phosphorus in carbon nanotube-backboned mesoporous carbon as superior anode material for sodium/potassium-ion batteries, Nano Energy, 52 (2018) 1-10.

[1] D.C. Marcano, D.V. Kosynkin, J.M. Berlin, A. Sinitskii, Z. Sun, A. Slesarev, L.B. Alemany, W. Lu, J.M. Tour, *ACS Nano*, **2010**, 8, 4806-4814.
[2] W. Tian, A. VahidMohammadi, Z. Wang, L. Ouyang, M. Beidaghi, M.M. Hamedi, *Nature Communications*, **2019**, 10, 2558.
[3] A. Sarycheva, Y. Gogotsi, *Chemistry of Materials*, **2020**, 32, 3480-3488.
[4] C.M. Subramaniyam, Z. Tai, N. Mahmood, D. Zhang, H.K. Liu, J.B. Goodenough, S.X. Dou, *Journal of Materials Chemistry A*, **2017**, 5, 1925-1929.

[5] S. Zhang, H. Liu, B. Cao, Q. Zhu, P. Zhang, X. Zhang, R. Chen, F. Wu, B. Xu, *Journal of Materials Chemistry A*, **2019**, 7, 21766-21773.

[6] R. Meng, J. Huang, Y. Feng, L. Zu, C. Peng, L. Zheng, L. Zheng, Z. Chen, G. Liu, B. Chen, Y. Mi, J. Yang, *Advanced Energy Materials*, **2018**, 8, 1801514.

[7] S.A. Ansari, M.H. Cho, *Scientific Reports*, **2016,** 6, 25405.

[8] S. Zhang, H. Ying, R. Guo, W. Yang, W.-Q. Han, *The Journal of Physical Chemistry Letters,* **2019**, 10, 6446-6454.

[9] T. Zhang, X. Jiang, G. Li, Q. Yao, J.Y. Lee, *ChemNanoMat*, **2018**, 4, 56-60.

[10] R. Zhao, Z. Qian, Z. Liu, D. Zhao, X. Hui, G. Jiang, C. Wang, L. Yin, *Nano Energy*, **2019**, 65, 104037.

[11] S. Zhang, X.-Y. Li, W. Yang, H. Tian, Z. Han, H. Ying, G. Wang, W.-Q. Han, *ACS Applied Materials & Interfaces*, **2019**, 11, 42086-42093.

[12] H. Li, A. Liu, X. Ren, Y. Yang, L. Gao, M. Fan, T. Ma, *Nanoscale*, **2019**, 11, 19862-19869.

[13] X. Guo, W. Zhang, J. Zhang, D. Zhou, X. Tang, X. Xu, B. Li, H. Liu, G. Wang, *ACS Nano*, **2020**, 14, 3651-3659.

[14] K. Fang, D. Liu, X. Xiang, X. Zhu, H. Tang, D. Qu, Z. Xie, J. Li, D. Qu, *Nano Energy*, **2020**, 69, 104451.

[15] X. Wu, W. Zhao, H. Wang, X. Qi, Z. Xing, Q. Zhuang, Z. Ju, *Journal of Power Sources*, **2018**, 378, 460-467.

[16] P. Xiong, P. Bai, S. Tu, M. Cheng, J. Zhang, J. Sun, Y. Xu, *Small*, **2018**, 14, 1802140.

[17] I. Sultana, M.M. Rahman, T. Ramireddy, Y. Chen, A.M. Glushenkov, *Journal of Materials Chemistry A*, **2017**, 5, 23506-23512.

[18] W.-C. Chang, J.-H. Wu, K.-T. Chen, H.-Y. Tuan, *Advanced Science*, **2019**, 6, 1801354.

[19] D. Liu, X. Huang, D. Qu, D. Zheng, G. Wang, J. Harris, J. Si, T. Ding, J. Chen, D. Qu, *Nano Energy*, **2018**, 52, 1-10.

[20] John F. Moulder, William F. Stickle, Peter E. Sobol, Kenneth D. Bomben, Handbook of X-ray Photoelectron Spectroscopy (1995)